Journal of
Materials Chemistry A

Materials for energy and sustainability

Accepted Manuscript

This article can be cited before page numbers have been issued, to do this please use: X. Guo, S. Chen, H. Wang, Z. Zhang, H. Lin, L. Song and T. Lu, *J. Mater. Chem. A*, 2019, DOI: 10.1039/C9TA06653E.

ROYAL SOCIETY OF CHEMISTRY

rsc.li/materials-a

View Article Online
DOI: 10.1039/C9TA06653E

ARTICLE

Single-Atom Molybdenum Immobilized on Photoactive Carbon Nitride as Efficient Photocatalysts for Ambient Nitrogen Fixation in Pure Water

Received 00th January 20xx,
Accepted 00th January 20xx

DOI: 10.1039/x0xx00000x

Xiang-Wei Guo,[‡a] Shuang-Ming Chen,[‡b] Hong-Juan Wang,[‡a] Zhi-Ming Zhang,*[a] Hong Lin,[a] Li Song[b] and Tong-Bu Lu*

A series of Mo single-atom catalysts were prepared by calcining low-cost primary material of urea with various amounts of $Na_2MoO_4{\cdot}2H_2O$. Isolated Mo centers are immobilized on in-situ formed polymeric carbon nitride via coordinating with two N donors to form two-coordinated MoN_2 species. The low-coordinated Mo centers can serve as active sites for N_2 chemisorption and activation, achieving high photocatalytic activity for NH_3 evolution with a rate of 50.9 μmol g_{cat}^{-1} h^{-1} in pure water. In the presence of ethanol as electron scavenger, the NH_3 evolution rate can reach to 830 μmol g_{cat}^{-1} h^{-1}, and the catalyst shows a quantum efficiency of 0.70% at 400 nm. This is the first single-atom catalyst that can drive photocatalytic N_2 fixation in pure water with comparable performance to recent reports for photocatalytic N_2 reduction. Experimental investigations and density functional theory calculations demonstrate that coordinatively unsaturated metal center in the single-atom catalysts can strongly adsorb N_2 via an end-on configuration to elongate the N≡N bond from 1.11 Å to 1.15 Å, thus photoexcited electrons can transfer to the weakened N≡N bond for efficient nitrogen fixation under ambient conditions. These findings provide new insight for solar-driven N_2 fixation by atomically dispersing low-coordination metal centers on photoactive supports.

Introduction

Ammonia synthesis from abundant N_2 in Earth's atmosphere represents a crucial and challenging chemical transformation to sustain all living organisms, as well as to generate potential carbon-free condensed fuels as the liquefiable feature of NH_3.[1-3] Up to date, industrial N_2 fixation through classical Haber-Bosch process and the biological ammonia synthesis are recognized as two most important and efficient strategies.[1] For Haber-Bosch process, this industrial N_2 fixation has to be conducted under rigorous reaction conditions (15–25 MPa, 573–823 K), consuming 1-3% of global energy supply,[4-6] and releasing a huge amount of greenhouse gas.[7,8] Its energy-intensive issue has motivated many scientists to explore alternative strategies for less-energy ammonia synthesis under ambient conditions, especially for solar-driven N_2 fixation as its highly attractive and great potential to sustainable energy solutions.[9,10]

Photocatalysis may provide a promising way by utilizing solar energy for N_2 fixation, which can supply photoexcited electrons to activate N≡N bond for the NH_3 synthesis (N_2 + $3H_2O$ → $2NH_3$ + $3/2O_2$).[11-18] However, photocatalytic NH_3 synthesis is still largely hampered as the poor binding between N_2 and photocatalysts, resulting in inefficient electron transfer from catalyst to the lowest unoccupied molecular orbital (LUMO) of N_2. As a result, the prerequisite for N_2 fixation is to construct electron-rich CUMCs for chemisorption of N_2 to build a bridge between N_2 and semiconductor. Recently, subtly designed defects in photocatalysts to create CUMCs with low-valence state has attracted wide attention.[19-24] In this field, numerous pioneering works, for instance, a series of photocatalysts BiOBr,[20] Bi_5O_7Br,[21] Layered-Double-Hydroxide[22] and Mo-doped $W_{18}O_{49}$[23] with CUMCs, have been performed to promote the chemisorption and activation of N_2. This progress guides scientists to devote to introducing ultra low-coordinated metal centers into photocatalysts to boost NH_3 evolution.

Recently, single-atom catalysts (SACs) with extremely exposed metal centers are widely concerned in heterogeneous catalysis as their unique catalytic activity and maximum of atom efficiency.[25-36] For N_2 fixation, first-principles calculations have proposed SACs as ideal catalysts for solar-driven N_2 fixation.[37] However, single atom (SA) photocatalysts were rarely explored. Presently, only atomically dispersed Cu and Fe anchored on polymeric carbon nitride (PCN) were constructed for photocatalytic N_2 reduction with ethanol as electron

[a] Institute for New Energy Materials & Low Carbon Technologies, School of Materials Science and Engineering, Tianjin University of Technology, Tianjin 300384, P. R. China. E-mail: zmzhang@email.tjut.edu.cn; lutongbu@mail.sysu.edu.cn.
[b] National Synchrotron Radiation Laboratory, CAS Center for Excellence in Nanoscience, University of Science and Technology of China, Hefei, Anhui 230029, P. R. China.

†Electronic Supplementary Information (ESI) available: [details of any supplementary information available should be included here]. See DOI: 10.1039/x0xx00000x

‡ The authors contributed equally to this work.

View Article Online
DOI: 10.1039/C9TA06653E

scavengers, affording the NH_3 evolution rate of 186 and 300 μmol g_{cat}^{-1} h^{-1}, respectively.[38,39] As well known, Mo element has played critical role for N_2 fixation in the most abundant nitrogenise,[40] and scientists have made great efforts to explore Mo-based catalysts for artificial synthesis of NH_3 under less-energy conditions.[23,41-42] Anchoring ultra low-coordinated SA Mo on photoactive support, that can utilize solar energy to replace the hydrolysis of ATP in organisms, may represent a possible alternative to nitrogenise for ambient N_2 fixation. Nevertheless, this remains an urgent and great challenge. Up to date, SA photocatalysts for N_2 fixation in pure water has yet to be achieved.[43]

Based on above consideration, we achieved a facile and large-scale synthesis of Mo-based SA photocatalysts (Mo-PCN) with low-coordinated MoN_2 species as active sites for N_2 fixation. The two-coordinated Mo centers in Mo-PCN can effectively adsorb N_2 and transfer enriched photoexcited electrons to the weakened N≡N bond, achieving efficient NH_3 production with a rate of 50.9 μmol g_{cat}^{-1} h^{-1} in pure water, and as high as 830 μmol g_{cat}^{-1} h^{-1} with ethanol as an electron scavenger. To our knowledge, this is the first SAC for photocatalytic N_2 fixation in pure water, which exhibits comparable performance to recent reports for photocatalytic N_2 reduction (Table S1).

Results and discussion

A series of Mo-PCN SACs (1-, 2- and 3-Mo-PCN) were facilely prepared by calcining a low-cost mixture of urea with various amounts of $Na_2MoO_4{\cdot}2H_2O$ at 450 °C (Figure S1). The urea can in situ transform to photoactive PCN,[44-46] which was used to stabilize SA Mo centers. High resolution transmission electron microscopy (HRTEM) image demonstrates that Mo-PCN shows similar morphology with that of pure PCN, and no Mo-based

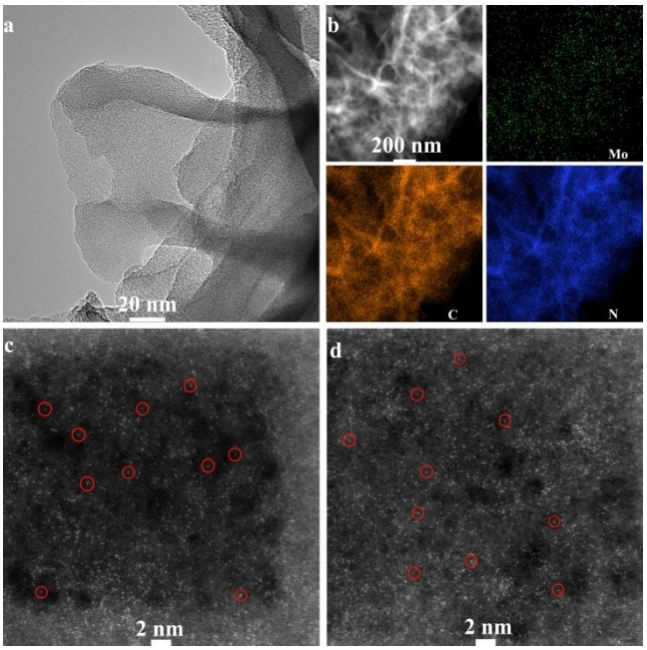

Figure 1. (a) HRTEM and (b) elemental mapping images of 3-Mo-PCN. Atomic-resolution HAADF-STEM images of 3-Mo-PCN (c) before and (d) after recycling tests, isolated Mo centers are marked with red circles.

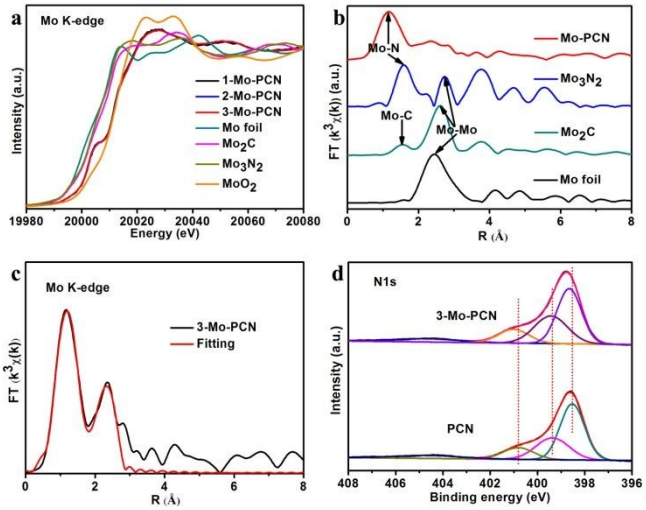

Figure 2. (a) XANES and (b) FT-EXAFS curves of Mo-PCN and references at Mo Kedge. (c) FT-EXAFS fitting curves of 3-Mo-PCN at Mo Kedge. (d) N 1s XPS spectra of PCN and 3-Mo-PCN.

nanoparticles can be observed in Mo-PCN (Figure 1a, S2-S4). Elemental mapping analysis reveals the homogeneous distribution of Mo, C and N elements over the SACs (Figure 1b, S5 and S6). These findings are consistent with the powder X-ray diffraction (PXRD) results, where only the humps of PCN were observed (Figure S7). Further, infrared spectroscopy (IR) spectra also show no obvious change of PCN after loading SA Mo centers (Figure S8). In Mo-PCN, SA Mo centers can be obviously discerned by atomic-resolution high angle annular dark-field scanning TEM (HAADF-STEM) imaging, where Mo SAs were confirmed by individual bright dots circled with red circles (Figure 1c and 1d, Figure S9 and S10). More than 99.5% Mo species on PCN show the size less than 0.2 nm (Figure S11), demonstrating the SA dispersion of Mo centers, and the Mo contents were determined by inductively coupled plasma mass spectrometry (ICP-MS) to be 0.109, 0.231 and 0.346 wt% in 1-, 2- and 3-Mo-PCN, respectively (Figure S12).

To further determine the local structure of Mo-PCN, extended X-ray absorption fine structure (EXAFS) and X-ray absorption near-edge structure (XANES) were performed. In the XANES curves (Figure 2a and S13), the absorption edge energy of these SACs all between those of Mo foil and MoO_2 references, revealing the positive low oxidation state of Mo SA center. As shown in Figure 2b, only one obvious FT peak was observed at ca. 1.2 Å in the FT-EXAFS curves of 3-Mo-PCN, which was mainly attributed to the scattering of Mo-N coordination. Meanwhile, no obvious Mo-Mo scattering peaks were observed, confirming the atomic dispersion of Mo centers on PCN, further supporting the HAADF-STEM observation (Figure 1c). Quantitative EXAFS fitting reveals that the Mo center was individually anchored on PCN via two Mo-N coordination bonds (Figure 2c, S14 and S15, Table S3). Additionally, one O_2 molecule was considered to be adsorbed

View Article Online
DOI: 10.1039/C9TA06535E

on Mo-PCN (Table S2). Further, with increasing the Mo content, the intensities of peaks A in N and C K-edge spectra (at 397.1 and 286.6 eV, respectively) decrease obviously as the reduction in number of π* bonds (Figure S15). This result indicates that introducing Mo centers can locally alter the electronic structure of PCN matrix.[34] X-ray photoelectron spectroscopy (XPS) characterization was also carried out to examine the electronic structure change of PCN after Mo loading (Figure 2d and S16). After loading SA Mo, the peak at 398.6 eV assigned to sp^2 hybridized aromatic N in C=N–C shifts to higher–energy at a certain extent, while no obvious change was observed towards the peaks of tertiary N in N–(C)3, the N in aromatic cycles bonded to three carbon atoms and π excitations at 399.7, 401.1 and 404.6 eV, respectively (Figure 2d).[34,47] These observations demonstrate the coordination of N in C=N–C with SA Mo centers, which can reduce the electron density of N atom via the formation of Mo-N bonds, being consistent with the result of EXAFS analysis (Figure S17).

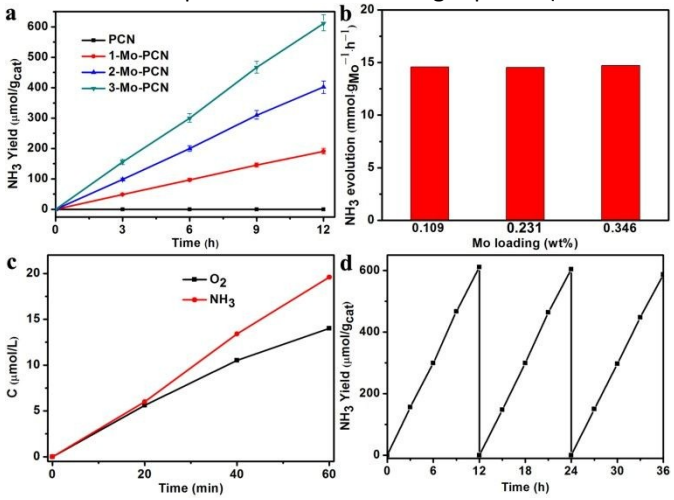

Figure 3. (a) Time course of NH_3 evolution in the photofixation of N_2 in pure water under 300 W Xenon lamp illumination. (b) Photocatalytic NH_3 evolution rate of SACs with various Mo contents normalized to Mo. (c) Photocatalytic oxygen evolution in the 3-Mo-PCN-containing photocatalytic system. (d) Recycling tests for 3-Mo-PCN with N_2 in pure water under 300 W Xe lamp illumination.

The catalytic activity for N_2 fixation of Mo-PCN was evaluated in double distilled water with different pH values under 300 W Xenon lamp irradiation, indicating that these SACs are most active in pH 5 water (Figure S18). During a typical process, SAC was dispersed in N_2-saturated water, which can directly serve as the source of electron and proton for NH_3 production. Upon the irradiation, NH_3 formed immediately, while the bare PCN was inactive (Figure 3a). The activity of the SACs exhibits an approximately linear growth with increasing the Mo contents, and total NH_3 generation outputs in pure water for 1-, 2- and 3-Mo-PCN within 12 h are 190.7, 402.8 and 611.2 μmol g_{cat}^{-1}, respectively (Figure 3a, S19). The NH_3 yield was double checked by the ion chromatograph (IC), which shows comparable results to those determined by Nessler's reagent (Table S3). In the presence of ethanol as an electron scavenger, the NH_3 evolution rate of 3-Mo-PCN was as high as 830 μmol g_{cat}^{-1} h^{-1}, with the experimental turnover number (TON) of 276 towards Mo centers, and the catalyst shows a quantum efficiency of 0.70% at 400 nm. Figure 3b gave the relative mass activity on per gram of Mo. Clearly, these SACs exhibit almost a constant mass activity of ca. 14.7 mmol g_{Mo}^{-1} h^{-1} in pure water, implying that each isolated Mo center is competent for catalytic N_2-to-NH_3 conversion. These results confirm the reliability of the NH_3 production, and these SACs with only 0.109-0.346 wt% Mo contents exhibit comparable activity to recent reports for photocatalytic N_2 reduction (Table S1). Also, the NH_3 evolution rate can reach to as high as 239 mmol g_{Mo}^{-1} h^{-1} with ethanol as an electron scavenger. In the photocatalytic process, negligible H_2 or N_2H_4 can be detected in the photocatalytic products (Figure S20), indicating a high selectivity for NH_3 formation in the aqueous phase. Further, the ^{15}N-labelling experiment was carefully performed, and the product was identified by ^1H NMR spectra. As shown in Figure S21, the doublet pattern with coupling constant of J_{N-H} = 72 Hz, corresponding to $^{15}NH_4^+$ in the acidic solution, can be obviously observed, revealing that the produced NH_3 indeed derives from N_2 fixation.[23,47] This result was reaffirmed by the control experiments, where no NH_4^+ can be detected under Ar, with PCN as the catalyst or in the dark (Figure S22 and Table S4). During N_2 fixation, O_2 evolution was detected with a yield close to 3/4 of NH_3 at the initial reaction stages (Figure 3c). This is a strong evidence that water molecule can act as the source of electron for NH_3 formation. 3-Mo-PCN also displays excellent stability with a constant NH_3 formation rate after three cyclic tests (Figure 3d). Further, 3-Mo-PCN retains its pristine morphology, and no aggregation of SA Mo centers can be observed after three successive catalytic cycles (Figure 1d, S23 and S24), demonstrating outstanding durability of Mo-PCN SACs. Based on above experiments, the origin of N atoms from the decomposition of PCN can be excluded, confirming that N_2, H_2O and light are all necessary for the NH_3 formation.

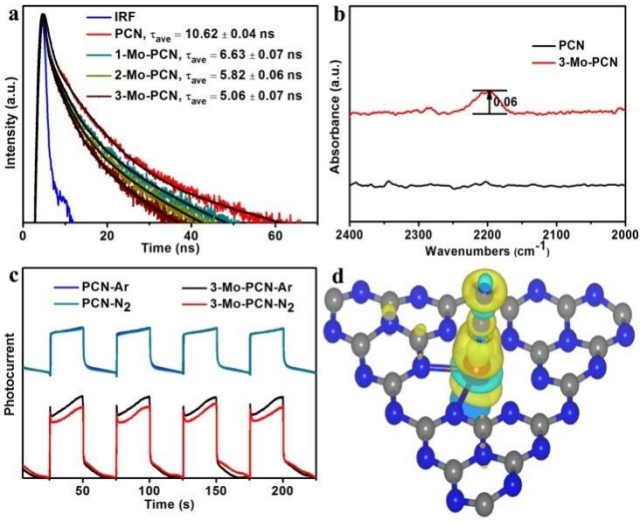

Figure 4. (a) Time-resolved fluorescence kinetics at 298 K. (b) LT-FTIR spectra after N_2 adsorption at 80 K. (c) Transient photocurrent responses of PCN and 3-Mo-PCN in N_2 and Ar atmosphere. (d) Charge density difference of Mo-PCN with adsorbed N_2, the yellow and cyan isosurfaces represent charge depletion and charge

accumulation, respectively (carbon, grey; nitrogen, blue; molybdenum, purple).

Steady and time-resolved fluorescence were performed to verify the transfer of photoexcited electron from PCN to Mo SA. Compared with bare PCN, the photoluminescence intensity of a broad PL band around 450 nm for Mo-PCN becomes much lower with increasing amounts of Mo loading (Figure S25). Time-resolved fluorescence kinetics measurements also reveal that the average radiative lifetimes reduce obviously in an order of PCN (10.62 ns) > 1-Mo-PCN (6.63 ns) > 2-Mo-PCN (5.82 ns) > 3-Mo-PCN (5.06 ns) (Figure 4a), indicating efficient transfer of photoexcited electron from PCN to Mo center to enhance the separation efficiency of photoinduced electron-hole pairs.

To determine the status of absorbed N_2 on Mo SA centers, Low-temperature Fourier transform infrared (LT-FTIR) spectroscopy and temperature-programmed desorption (TPD) measurements were further performed. After N_2 adsorption, the LT-FTIR spectra of 3-Mo-PCN shows a broad peak at 2197 cm^{-1} (Figure 4b), corresponding to adsorbed N_2 molecules on Mo centers with an end-on configuration.[7] In the TPD experiment, the desorption peak of chemisorbed N_2 was only obviously observed on Mo-PCN SAC (Figure S26), indicating the chemical adsorption of N_2 on SA Mo center in the SAC. In addition, the interfacial charge kinetics for PCN and 3-Mo-PCN were detected to investigate the electron transfer between SA Mo and absorbed N_2 via the transient photocurrent response experiments (Figure 4c). In this process, the photocurrent generated by transfer of photoexcited electrons to the electrode in N_2 atmosphere is lower than that obtained under Ar, due to the competitive interfacial electron transfer to chemisorbed N_2 molecules.[19,22] Moreover, compared with PCN, 3-Mo-PCN shows a significant reduced photocurrent, confirming favorable energetic electron transfer to the N≡N triple bond of chemisorbed N_2 via the SA center.

Density functional theory (DFT) calculations were conducted to better understand the catalytic process for N_2 reduction (Figure S27). It should be noted that the side-on mechanism is not considered here, as its configuration on SA Mo is not stable. Also, the LT-FTIR experiments confirm the end-on configuration of the absorbed N_2 molecules (Figure 4b). For the end-on configuration, DFT calculations demonstrate that only physical adsorption exists between pure PCN and N_2 molecule. The distance between adsorbed N_2 and bare PCN is approximately 3.30 Å, and the N≡N bond length is the same as that of isolated N_2 molecule. For Mo-PCN, the Mo center can bind N_2 and H_2O molecule with an adsorption energy of -1.31 eV and -0.391 eV, respectively, implying a stronger chemical adsorption between Mo center and N_2 molecule. When N_2 molecule approaches Mo center, a Mo-N coordination bond was formed with a distance of 1.90 Å (Figure S28). Meanwhile, the N···N distance was elongated from 1.11 Å to 1.15 Å, indicating the N≡N bond is weaken via the formation of Mo-N≡N. For the photocatalytic N_2 reduction, there are two reaction mechanisms for the end-on configuration, the distal (M^n–N≡N → M^{n+3}≡N + NH_3 → M^n + NH_3) and alternating (M^n–N≡N → M^n–NH=NH → M^n–NH_2–NH_2→ M^n + $2NH_3$) mechanisms (Figure S29).[38-41] In both distal and alternating mechanisms, there is an identical process that the adsorbed N_2 binds one proton coupled with an electron transfer to form N_2H^* intermediate. Further, three protons are consecutively added to the distal N atom to release one NH_3 molecule for the distal process. While for the alternating process, the protons were alternately added to two N atoms in a N_2 molecule, releasing the first NH_3 molecule until the fifth proton was adsorbed. As shown in Figure S27, the rate determining step for both distal and alternating processes is the transformation of N_2 to N_2H^*, which is an endothermic process requiring an energy barrier of 0.81 eV. These results imply that two reaction pathways can simultaneously exist in the photocatalytic N_2 fixation process.

Conclusions

In conclusion, we have developed a facile and large-scale synthetic strategy to construct Mo-PCN SA photocatalysts for N_2 reduction to NH_3, through calcining cheap urea with various amounts of $Na_2MoO_4{\cdot}2H_2O$. Various investigations demonstrate for the first time that the resulting two-coordinated Mo center can strongly adsorb N_2 via an end-on configuration to elongate the N≡N bond from 1.11 to 1.15 Å to weaken the N≡N bond. Further, the CUMCs in Mo-PCN SACs can act as a bridge to accept photoexcited electrons from PCN, and donate the energetic electrons to N≡N triple bond to achieve efficient N_2 reduction at ambient conditions. The photocatalytic NH_3 production was first achieved with SACs using water as a reducing agent, and the NH_3 evolution rate can reach as high as 14.7 mmol g_{Mo}^{-1} h^{-1} (50.9 μmol g_{cat}^{-1} h^{-1}). This work provides new insight for solar-driven nitrogen fixation by atomically dispersing low-coordination transition metal centers on photoactive supports.

Experimental

Materials

$Na_2MoO_4{\cdot}2H_2O$ (AR. ≥ 99.0%), urea (AR. ≥ 99.0%) and ethanol (AR. ≥99.7%) were purchased from Tianjin Fuchen Chemical Reagent Co. Ltd. (Tianjin, China). Hydrochloric Acid (HCl ~37%) was purchased from Sinopharm Chemical Reagent Co. Ltd. (Shanghai, China). Potassium sodium tartrate tetrahydrate (GR. 99.5%) and Ammonium chloride-^{15}N (10 atom%, ≥ 98.5%) were purchased from Shanghai Aladdin Bio-Chem Technology Co. LTD. (Shanghai, China). Nessler's reagent was purchased from Beijing Innochem Science & Technology Co. LTD. (Beijing, China). DMSO-d_6 was purchased from Cambridge Isotope Laboratories, Inc. (Andover, MA, USA). $^{15}N_2$ (>99 atom%) was purchased from China Dalian Delin Gas Packing co., Ltd. (Dalian, China). Double distilled water was used in all the experiments.

Characterization

XRD patterns were collected using a Rigaku Smartlab 9 KW diffractometer. UV-Vis absorbance spectra were recorded on a PemkinElmer Lambda 750 UV/VIS/NIR spectrometer. FT-IR was recored on a PemkinElmer Frontier Mid-IR FTIR spectrometer.

View Article Online DOI: 10.1039/C9TA06655F

ICP-MS were recorded on a Agilent 7800. TEM and EDS characterizations were achieved using JEOL JEM-2100, FEI Talos F200X and FEI Titan Cubed Themis G2 300 with a probe corrector. XPS measurements were performed with a Thermal scientific ESCALAB250Xi system with the Al Kα radiation as the X-ray source. The amount of NH_4^+ in the solution was analysed by ion chromatography (DX-120, DIONEX) and Nessler's reagent. Low-temperature Fourier transform infrared spectroscopy (LT-FTIR) spectra were performed using a Bruker IFS 66v Fourier-transform spectrometer equipped with a mercury–cadmium–tellurium (MCT) detector at BL01B in NSRL in Hefei, China. Mo K-edge XAFS spectra were collected at the Shanghai Synchrotron Radiation Facility (BL14W1, SSRF). The X-ray was mono-chromatized by a double-crystal Si (311) monochromator for SSRF. The acquired EXAFS data were processed according to the standard procedures using the WinXAS3.1 program.[48] Theoretical amplitudes and phase-shift functions were further calculated with the FEFF8.2.[49]

Synthesis of Polymeric Carbon Nitride (PCN)

PCN was synthesized by calcining urea at 450 ℃ for 3 h (ramp rate, 5 ℃/min) in a crucible with a cap. The capped crucible was placed in the muffle furnace under the air atmosphere. After cooling to room temperature, the yellow product was washed with double distilled water and ethanol, and subsequently dried at 80 ℃ for 12 h.

Synthesis of Mo-PCN SACs

4 g urea was dissolved in 16 mL double distilled water, followed by the addition of 1, 2 or 3 mg of $Na_2MoO_4{\cdot}2H_2O$ into this aqueous solution. The resulting mixture was stirred for 3 h at room temperature to ensure the uniform dispersion. Then, the water was removed by rotary evaporator. The resulting white product was calcined at 450 ℃ (ramp rate, 5 ℃/min) for 3 h in a muffle furnace. The obtained yellow product was washed with 1 M HCl, double distilled water and ethanol, and subsequently dried at 80 ℃ for 12 h. The yellow products were named as 1-, 2- and 3-Mo-PCN, respectively. Also, this facile experimental procedure can be easily enlarged by changing the dosage of urea/$Na_2MoO_4{\cdot}2H_2O$. As a result, 20 g urea with 5 mg, 10 mg and 15 mg of $Na_2MoO_4{\cdot}2H_2O$ can be used to synthesize 1-, 2- and 3-Mo-PCN, respectively, limited by the space of muffle furnace in the lab.

Photocatalytic Reaction

3 mg of photocatalyst was added to 6 mL double distilled water within a quartz reactor, and dispersed well by ultrasonication (60 min). The pH value of the photocatalytic system was adjusted with 0.1 M HCl. The reactor was equipped with a recycled water to maintain the room temperature. High-purity N_2 was bubbled into the solution in dark with stirring for 60 min to obtain a N_2-saturated aqueous suspension. Then, the reactor was irradiated using the 300 W Xe lamp (PLS-SXE300D) for 12 h.

The Methods for NH_4^+ Detection

The concentration of ammonia was measured by a colorimetric method with Nessler's reagent.[50-53] After the photocatalytic reaction, the suspension was centrifuged, and the solution was filtered through a 220 nm membrane filter. To make sure the absorbance for each solution is within the linear range of the calibration curve, the filtrate after the photocatalytic reaction was diluted five times with double distilled water. Then, 100 μL of potassium sodium tartrate solution was added to 5 mL of the above solution. After blending, 150 μL of Nessler's reagent was added to this solution, which was left to stand for 30 min for full color processing (Figure S31). The concentration of NH_4^+ was determined using an UV-vis spectrophotometer at 420 nm. Calibration curves for NH_3 assay using Nessler's reagent (R^2 = 0.9997) showed highly linear responses with the concentration of NH_4^+ in the concentration range of 0-2000 μg/L (Figure S32a).

The concentration of ammonia was also measured by ion chromatography method. Ion chromatography for a series of reference solutions with suitable NH_4Cl concentrations (0.50, 1.0, 1.5, and 2.0 μg/mL) were acquired and a calibration curve (R^2 = 0.9996)) was plotted (Figure S32b). The filtrate after the photocatalytic reaction was acidized with 0.1 M HCl and then measured by ion chromatography method.

The ammonia production rates with different detection methods was shown in Table S2, which supplied similar results with the detected NH_3 concentration matching closely.

Determination of Apparent Quantum Efficiency

In this process, LED light (λ = 400 nm, 100 mW·cm^{-2}, irradiation area 0.8 cm^2) was utilized as a monochromatic light source. The quantum efficiency at 400 nm was calculated on the basis of the following equation: quantum efficiency = 100% × (number of generated ammonia × 3 / number of incident photons at 25 °C). The quantum efficiency of 3-Mo-PCN at 400 nm was determined to be 0.7% in the presence of ethanol as electron scavenger.

Isotope-labeled Experiments

An isotopic labeling experiment used $^{15}N_2$ as the feeding gas to clarify the nitrogen source of ammonia. After the photocatalytic reaction, the obtained filtrate was then mixed with 20% DMSO-d_6. NMR measurements were then performed on a Bruker III HD 400 MHz system. The standard solution of NH_4Cl with ^{15}N enrichment of 10% was further detected by ^{1}HNMR to confirm the generation of $^{15}NH_4^+$ during the photocatalytic process.[54-56]

N_2-Temperature-Programmed Desorption (TPD) Measurements

TPD measurements were performed to understand N_2 adsorption on the surface of PCN and 3-Mo-PCN. Typically, the sample was placed in a glass tube, and was pretreated by He gas flow at 300 °C for 2 h, and then cooled down to 50 °C. The adsorption of N_2 was conducted in a 99.999% N_2 gas fow for 1 h at 50 °C. After purging with He gas for 1 h to remove the residual N_2, the sample was heated from 50 °C to 400 °C at a rate of 10 °C min^{-1}. The TPD signal was recorded using a thermal conductivity detector (TCD). The N_2-TPD measurements were performed on a chemisorption apparatus (Micromeritics AutoChem II 2920).

Computational Details

The first-principles calculations were performed by using the Vienna *ab initio* simulation package (VASP) based on the spin-polarized density functional theory.[57,58] The generalized gradient approximation (GGA) of Perdew-Burke-Ernzerh (PBE) was adopted for the exchange-correlation function.[59] And the electron-ion interaction was described by the projected augmented wave (PAW) method.[60] The electronic wave functions were expanded by a plane wave basis set with an energy cutoff of 450 eV. The van der Waals interactions were described using DFT-D3 method with Becke-Jonson damping.[61] A 2 × 2 × 1 supercell PCN contains 32 N atoms and 24 C atoms was selected as the slab model. In order to avoid the interaction between two layers, the vacuum layers were set to be 15 Å. During the calculations, the Brillouin zones were sampled by a 3 × 3 × 1 grid centered at the gamma (Γ) point, all the atoms were fully relaxed until the total energy variation was smaller than 10^{-5} eV, and the force on each atom was less than 0.02 eV/ Å. The Gibbs free energy change (ΔG) in the simulated pathway was calculated as follows:

$$\Delta G = \Delta E + \Delta E_{ZPE} - T\Delta S$$

Where, ΔE is the adsorption energy difference obtained directly from DFT calculations, ΔE_{ZPE} is the difference in zero point energy computed from the vibrational frequencies, *T* is the temperature (298.15 K), and ΔS is the entropy difference between the adsorbed state and gas state. As the vibrational entropy of the adsorbed state is small, it is neglected. While the entropies for the gas molecules are taken from the NIST database.[62]

Conflicts of interest

There are no conflicts to declare.

Acknowledgements

This work was supported by National Key R&D Program of China (2017YFA0700104), the National Natural Science Foundation of China (21722104, 21671032, 21331007), and Natural Science Foundation of Tianjin City of China (18JCJQJC47700, 17JCQNJC05100).

Notes and references

1 J. W. Erisman, M. A. Sutton, J. Galloway, Z. Klimont and W. Winiwarter, *Nat. Geosci.,* 2008, **1**, 636-639.
2 V. Rosca, M. Duca, M. T. Groot and M. T. M. Koper, *Chem. Rev.,* 2009, **109**, 2209-2244.
3 H. Jia and E. A. Quadrelli, *Chem. Soc. Rev*., 2014, **43**, 547-564.
4 K. Honkala, A. Hellman, I. N. Remediakis, A. Logadottir, A. Carlsson, S. Dahl, C. H. Christensen and J. K. Nørskov, *Science,* 2005, **307**, 555-558.
5 S. Licht, B. Cui, B. Wang, F. Li, J. Lau and S. Liu, *Science,* 2014, **345**, 637-640.
6 J. M. P. Martirez and E. A. Carter, *J. Am. Chem. Soc.,* 2017, **139**, 4390-4398.
7 M. Kitano, Y. Inoue, Y. Yamazaki, F. Hayashi, S. Kanbara, S. Matsuishi, T. Yokoyama, S-W. Kim, M. Hara and H. Hosono, *Nat. Chem.,* 2012, **4**, 934-940.
8 C. J. M. V. Ham, M. T. M. Koper and D. G. H. Hetterscheid, *Chem. Soc. Rev.,* 2014, **43**, 5183-5191.
9 A. J. Medford and M. C. Hatzell, *ACS Catal.,* 2017, **7**, 2624-2643.
10 X. Chen, N. Li, Z. Kong, W-J. Ong and X. Zhao, *Mater. Horiz.*, 2018, **5**, 9-27.
11 D. Zhu, L. Zhang, R. E. Ruther and R. J. Hamers, *J. Nat. Mater.,* 2013, **12**, 836.
12 T. Oshikiri, K. Uenoand H. Misawa, *Angew. Chem. Int. Ed.,* 2014, **53**, 9802.
13 M. Ali, F. Zhou, K. Chen, C. Kotzur, C.. Xiao, L. Bourgeois, X. Zhang and D. R. MacFarlane, *Nat. Commun.,* 2016, **7**, 11335.
14 K. A. Brown, D. F. Harris, M. B. Wilker, A. Rasmussen, N. Khadka, H. Hamby, S. Keable, G. Dukovic, J. W. Peters, L. C. Seefeldt and P. W. King, *Science,* 2016, **352**, 448-450.
15 J. Zheng, Y. Lyu, M. Qiao, R. Wang, Y. Zhou, H. Li, C. Chen, Y. Li, H. Zhou, S. Jiang and S. Wang, *Chem,* 2019, **5**, 617-633.
16 L. F. Greenlee, J. N. Renner and S. L. Foster, *ACS Catal.,* 2018, **8**, 7820-7827.
17 S. D. Minteer, P. Christopher and S. Linic, *ACS Energy Lett.,* 2019, **4**, 163-166.
18 C. Hu, X. Chen, J. Jin, Y. Han, S. Chen, H. Ju, J. Cai, Y. Qiu, C. Gao, C. Wang, Z. Qi, R. Long, L. Song, Z. Liu and Y. Xiong, *J. Am. Chem. Soc.*, 2019, **141**, 7807.
19 G. N. Schrauzer and T. D. Guth, *J. Am. Chem. Soc.,* 1977, **99**, 7189-7193.
20 H. Li, J. Shang, Z. Ai and L. Zhang, *J. Am. Chem. Soc*., 2015, **137**, 6393-6399.
21 S. Wang, X. Hai, X. Ding, K. Chang, Y. Xiang, X. Meng, Z. Yang, H. Chen and J. Ye, *Adv. Mater.,* 2017, **29**, 1701774.
22 Y. Zhao, Y. Zhao, G. I. N. Waterhouse, L. Zheng, X. Cao, F. Teng, L. Wu, C-H. Tung, D. O'Hare and T. Zhang, *Adv. Mater.,* 2017, **29**, 1703828.
23 N. Zhang, A. Jalil, D. Wu, S. Chen, Y. Liu, C. Gao, W. Ye, Z. Qi, H. Ju, C. Wang, X. Wu, L. Song, J. Zhu and Y. Xiong, *J. Am. Chem. Soc.,* 2018, **140**, 9434-9443.
24 L. Tao, M. Qiao, R. Jin, Y. Li, Z. Xiao, Y. Wang, N. Zhang, C. Xie, Q. He, D. Jiang, G. Yu, Y. Li and S. Wang, *Angew. Chem. Int. Ed.,* 2019, **58**, 1019-1024.
25 X. Yang, A. Wang, B. Qiao, J. Li, J. Liu and T. Zhang, *Acc. Chem. Res.,* 2013, **46**, 1740-1748.
26 H. Tao, C. Choi, L. Ding, Z. Jiang, Z. Han, M. Jia, Q. Fan, Y. Gao, H. Wang, A. W. Robertson, S. Hong, Y. Jung, S. Liu and Z. Sun, *Chem,* 2019, **5**, 204-214.
27 J. Wang, Z. Li, Y. Wu and Y. Li, *Adv. Mater.,* 2018, **30**, 1801649.
28 W. Chen, J. Pei, C. He, J. Wan, H. Ren, Y. Zhu, Y. Wang, J. Dong, S. Tian, W. Cheong, S. Lu, L. Zheng, X. Zheng, W. Yan, Z. Zhuang, C. Chen, Qi. Peng, D. Wang and Y. Li, *Angew. Chem. Int. Ed*., 2017, **56**, 16086-16090.
29 Z. Geng, Y. Liu, X. Kong, P. Li, K. Li, Z. Liu, J. Du, M. Shu, R. Si and J. Zeng, *Adv. Mater.,* 2018, **30**, 1803498.
30 B. Wang, H. Cai and S. Shen, *Small Methods,* 2019, 1800447.
31 C. Choi, S. Back, N.-Y. Kim, J. Lim, Y.-H. Kim and Y. Jung, *ACS Catal.,* 2018, **8**, 7517-7525.
32 X. Guo, G. Fang, G. Li, H. Ma, H. Fan, L. Yu, C. Ma, X. Wu, D. Deng, M. Wei, D. Tan, R. Si, S. Zhang, J. Li, L. Sun, Z. Tang, X. Pan and X. Bao, *Science,* 2014, **344**, 616-619.
33 W. Liu, L. Cao, W. Cheng, Y. Cao, X. Liu, W. Zhang, X. Mou, L. Jin, X. Zheng, W. Che, Q. Liu, T. Yao and S. Wei, *Angew. Chem. Int. Ed.,* 2017, **56**, 9312-9317.
34 X. Li, W. Bi, L. Zhang, S. Tao, W. Chu, Q. Zhang, Y. Luo, C. Wu and Y. Xie, *Adv. Mater.,* 2016, **28**, 2427-2431.
35 Y. Zheng, Y. Jiao, Y. Zhu, Q. Cai, A. Vasileff, L. Li, Y. Han. Y. Chen and S. Qiao, *J. Am. Chem. Soc*., 2017, **139**, 3336-3339.
36 L. Fan, P. Liu, X. Yan, L. Gu, Z. Yang, H. Yang, S. Qiu and X. Yao, *Nat. Commun.,* 2016, **7**, 10667.

View Article Online
DOI: 10.1039/C9TA06653E

37 C. Ling, X. Niu, Q. Li, A. Du and J. Wang, *J. Am. Chem. Soc.,* 2018, **140**, 14161-14168.
38 P. Huang, W. Liu, Z. He, C. Xiao, T. Yao, Y. Zou, C. Wang, Z. Qi, W. Tong, B. Pan, S. Wei and Y. Xie, *Sci. China Chem*., 2018, **61**, 1187-1196.
39 S. Hu, X. Chen, Q. Li, F. Li, Z. Fan, H. Wang, Y. Wang, B. Zheng and G. Wu, *Appl. Catal. B: Environ.,* 2017, **201**, 58-69.
40 J. B. Howard and D. C. Rees, *PNAS,* 2006, **103**, 17088-17093.
41 J. Zhao and Z. Chen, *J. Am. Chem. Soc.,* 2017, **139**, 12480-12487.
42 D. Yang, T. Chen and Z. Wang, *J. Mater. Chem. A,* 2017, **5**, 18967-18971.
43 19. S. Liu, Y. Wang, S. Wang, M. You, S. Hong, T. Wu, Y. Soo, Z. Zhao, G. Jiang, J. Qiu, B. Wang and Z. Sun, *ACS Sustainable Chem. Eng.,* 2019, **7**, 6813.
44 F. K. Kessler, Y. Zheng, D. Schwarz, C. Merschjann, W. Schnick, X. Wang and M. J. Bojdys, *Nature Rev.,* 2017, **2**, 17030.
45 G. Zhang, L. Lin, G. Li, Y. Zhang, A. Savateev, S. Zafeiratos, X. C. Wang and M. Antonietti, *Angew. Chem. Int. Ed*., 2018, **57**, 9372-9376..
46 J. Liu, T. Zhang, Z. Wang, G. Dawsona and W. Chen, *J. Mater. Chem.,* 2011, **21**, 14398-14401..
47 J. Han, X. Ji, X. Ren, G. Cui, L. Li, F. Xie, H. Wang, B. Li and X. Sun, *J. Mater. Chem. A,* 2018, **6**, 12974-12977.
48 T. Ressler, *J. Synchrotron Radiat.* 1998, **5**, 118-122.
49 A. L. Ankudinov, B. Ravel, J. J. Rehr and S. D. Conradson, *Phys. Rev. B*., 1998, **58**, 7565-7576.
50 Y. Hao, Y. Guo, L. Chen, M. Shu, X. Wang, T. Bu, W. Gao, N. Zhang, X. Su, X. Feng, J. Zhou, B. Wang, C. Hu, A. Yin, R. Si, Y. Zhang and C. Yan, *Nature Catalysis*, 2019, **2**, 448-456.
51 X. Gao, Y. Wen, D. Qu, L. An, S. Luan, W. Jiang, X. Zong, X. Liu and Z. Sun, ACS Sustainable Chem. Eng., 2018, **6**, 5342-5348.
52 Y. Zhao, R. Shi, X. Bian, C. Zhou, Y. Zhao, S. Zhang, F. Wu, G. I. N. Waterhouse, L. Wu, C. Tung and T. Zhang, Adv. Sci., 2019, **6**, 1802109.
53 B. Hu, M. Hu, L. Seefeldt and T. Liu, ACS Energy Lett., 2019, **4**, 1053-1054
54 X. Zhu, Z. Liu, H. Wang, R. Zhao, H. Chen, T. Wang, F. Wang, Y. Luo, Y. Wu and X. Sun, *Chem. Commun.*, 2019, **55**, 3987-3990.
55 X. Zhang, T. Wu, H. Wang, R. Zhao, H. Chen, T. Wang, P. Wei, Y. Luo, Y. Zhang and X. Sun, *ACS Catal.*, 2019, **9**, 4609-4615.
56 T. Wang, L. Xia, J. Yang, H. Wang, W. Fang, H. Chen, D. Tang, A. M. Asiri, Y. Luo, G. Cui and X. Sun, *Chem. Commun.*, 2019, **55**, 7502-7505.
57 G. Kresse and J. Hafner, *Phys. Rev. B,* 1994, **49**, 14251-14269.
58 G. Kresse and J. Furthmüller, *Phys. Rev. B,* 1996, **54**, 11169-11186.
59 J. P. Perdew, K. Burke and M. Ernzerhof, *Phys. ReV. Lett*., 1996, **77**, 3865-3868.
60 P. E. Blöchl, *Phys. Rev. B,* 1994, **50**, 17953-17979.
61 S. Grimme, J. Antony, S. Ehrlich and H. Krieg, *J. Chem. Phys*., 2010, **132**, 154104.
62 Computational Chemistry Comparison and Benchmark Database.http://cccbdb.nist.gov/.